as being typical of the ionic state, whereas all the 200 K spectra showing the higher-lying peak (N; $\nu_N \sim 1430$ cm^{-1}, red curves) indicate the neutral state, with $\rho \sim 0.2$. The 4.2 K spectrum of the 2,6-QBr_2Cl_2 complex, located at the NI QCP, reveals a blurred feature, implying that the dynamic distribution of the molecular ionicity, or equivalently the valence fluctuation with the time scale, is comparable to $(\nu_N - \nu_I)^{-1} \sim 30$ ps (*25*). Hence, the quantum paraelectric behavior in the DMTTF complex should originate from the quantum valence fluctuation rather than from the simple displacive (anti)ferroelectric transition. The dynamics of NI domain walls along the *DA* stacks, which can be related to the gigantic dielectric response above T_c in the NI transition system (*26*), may experience quantum motion and cause the collective fluctuation of the molecular valence.

The critical behavior, analogous to quantum ferroelectrics, provides evidence for the quantum valence fluctuation in the organic CT complexes. The phase transition near $T = 0$ can be driven by hydrostatic or equivalent chemical pressure. Such an anomalous variation of the molecular valence at $T = 0$ has not been observed previously for any conventional quantum ferroelectrics, and the phase transition may be distinguished as a quantum NI transition.

References and Notes

1. J. S. Miller, Ed., *Extended Linear Chain Compounds* (Plenum Press, New York, 1982), vols. 1 to 3.
2. T. Ishiguro, K. Yamaji, G. Saito, Eds., *Organic Superconductors* (Springer-Verlag, Berlin, ed. 2, 1998).
3. E. Coronado, P. Delhaes, D. Gatteschi, J. S. Miller, Eds., *Molecular Magnetism: From Molecular Assemblies to the Devices*, vol. E321, *NATO ASI Series* (Kluwer Academic, Dordrecht, Netherlands, 1996).
4. K. Nasu, Ed., *Relaxations of Excited States and Photo-Induced Phase Transitions* (Springer-Verlag, Berlin, 1997).
5. J. B. Torrance, J. E. Vazquez, J. J. Mayerle, V. Y. Lee, *Phys. Rev. Lett.* **46**, 253 (1981).
6. Y. Tokura *et al., Phys. Rev. Lett.* **63**, 2405 (1989).
7. M. H. Lemée-Cailleau *et al., Phys. Rev. Lett.* **79**, 1690 (1997).
8. T. Luty *et al., Europhys. Lett.* **59**, 619 (2002).
9. N. D. Mathur *et al., Nature* **394**, 39 (1998).
10. Q. Si, S. Rabello, K. Ingersent, J. L. Smith, *Nature* **413**, 804 (2001).
11. S. A. Grigera *et al., Science* **294**, 329 (2001).
12. S. Aoki, T. Nakayama, A. Miura, *Phys. Rev. B* **48**, 626 (1993).
13. S. Horiuchi, Y. Okimoto, R. Kumai, Y. Tokura, *J. Am. Chem. Soc.* **123**, 665 (2001).
14. K. A. Müller, H. Burkard, *Phys. Rev. B* **19**, 3593 (1979).
15. G. A. Samara, *Phys. Rev. Lett.* **27**, 103 (1971).
16. J. H. Barrett, *Phys. Rev.* **86**, 118 (1952).
17. S. Horiuchi, Y. Okimoto, R. Kumai, Y. Tokura, data not shown.
18. S. Aoki, T. Nakayama, A. Miura, *Synth. Met.* **70**, 1243 (1995).
19. T. Mitani *et al., Phys. Rev. B* **35**, 427 (1987).
20. N. Nagaosa, *J. Phys. Soc. Jpn.* **55**, 2754 (1986).
21. Concerning the low-T phase of DMTTF-QCl_4 crystal, E. Collet *et al.* (*27*) recently reported the doubling of one interchain axis of the triclinic unit cell, which originally contains only one *DA* pair. Furthermore, their structural analysis showed a layered ferrielectric ordering of antiparallel *DA* dimer by assuming that two (nonequivalent) *N* and *I* layers alternate along this doubled axis (noncentrosymmetric space group *P*1). However, both infrared and Raman spectroscopy (Fig. 4) have provided evidence in support of the homogeneous ρ without the mode splitting that would be expected for the modulated molecular environment and/or ionicity in the presence of nonequivalent *DA* stacks. In accord with these spectroscopic results, our latest structural analysis by synchrotron x-ray diffraction ($\lambda = 0.699$ Å) on our DMTTF-QCl_4 specimen at 14 K ($<T_c$) successfully demonstrated that two equivalent *DA* dimers in a centrosymmetic supercell (space group $P\bar{1}$) construct a layer-type antiferroelectric order (*28*). {$R = 0.063$, $R_w = 0.066$, based on 1387 observed reflections [$I > 3\sigma(I)$] and 237 variable parameters.}
22. T. Schneider, H. Beck, E. Stoll, *Phys. Rev.* **B13**, 1123 (1976).
23. Y. Nogami *et al., Synth. Met.* **70**, 1219 (1995).
24. A. Girlando, I. Zanon, R. Bozio, C. Pecile, *J. Chem. Phys.* **68**, 22 (1978).
25. S. Horiuchi, Y. Okimoto, R. Kumai, Y. Tokura, *J. Phys. Soc. Jpn.* **69**, 1302 (2002).
26. Y. Okimoto *et al., Phys. Rev. Lett.* **87**, 187401 (2001).
27. E. Collet *et al., Phys. Rev. B* **63**, 054105 (2001).
28. Supplementary material is available on *Science* Online.
29. A. Girlando, R. Bozio, C. Pecile, J. B. Torrance, *Phys. Rev.* **B26**, 2306 (1982).

30. We thank H. Okamoto, N. Nagaosa, S. Miyasaka, N. Takeshita, Y. Ogawa, and H. Sawa for enlightening discussions.

Supporting Online Material

www.sciencemag.org/cgi/content/full/299/5604/229/DC1
SOM Text
Figs. S1 to S3
Tables S1 to S6

15 July 2002; accepted 20 November 2002

Bose-Einstein Condensation of Cesium

Tino Weber, Jens Herbig, Michael Mark, Hanns-Christoph Nägerl, Rudolf Grimm

Bose-Einstein condensation of cesium atoms is achieved by evaporative cooling using optical trapping techniques. The ability to tune the interactions between the ultracold atoms by an external magnetic field is crucial to obtain the condensate and offers intriguing features for potential applications. We explore various regimes of condensate self-interaction (attractive, repulsive, and null interaction strength) and demonstrate properties of imploding, exploding, and non-interacting quantum matter.

Cesium (Cs) is an atom of particular interest in physics. It serves as our primary frequency standard (*1*) and has various important applications in fundamental metrology, such as measurements of the fine-structure constant (*2*), the electric dipole moment of the electron (*3*), parity violation (*4*), and the Earth's gravitational field (*5*). Cs, a heavy alkali atom with small photon recoil, is well suited for laser cooling and trapping methods. However, because of quantum-mechanical scattering resonances, collisions between Cs atoms at ultralow energy exhibit unusual properties with drastic consequences, such as large frequency shifts in atomic clocks (*1*). A further consequence of this resonant scattering is the fact that Cs has so far resisted all attempts to produce Bose-Einstein condensation (BEC) (*6*–*13*). In contrast, all other stable alkali species—^{87}Rb (*14*), ^{23}Na (*15*), ^{7}Li (*16*), ^{85}Rb (*17*), and ^{41}K (*18*)—have been condensed, along with hydrogen (*19*) and metastable ^{4}He (*20*).

We report the achievement of BEC of Cs (^{133}Cs, the only stable isotope) using optical trapping methods in combination with magnetic tuning of the scattering properties. With the condensate, we explore the tunability of its self-interaction that results from low-field Feshbach resonances (*21*, *22*). Across such a Feshbach resonance, the *s*-wave scattering length a shows a dispersive variation as a function of the applied magnetic field from very large positive to negative values. The magnetic tunability of the self-interaction has been exploited in experiments with magnetically trapped ^{85}Rb (*17*) and optically trapped ^{7}Li (*23*, *24*). Cs offers further flexibility because of a unique combination of resonances at low magnetic fields: One broad Feshbach resonance allows for precise tuning, whereas several narrow resonances enable very rapid control. With the magnetic field being a free parameter in our optical trapping approach to BEC, we can take full advantage of this tunability. By switching a to zero, we realize a non-interacting condensate that undergoes minimum expansion when released from the trap. By variations of the magnetic field, we observe an imploding BEC at negative a, a gently expanding BEC at moderate positive values of a, and an exploding condensate on a narrow Feshbach resonance.

Early experiments attempting BEC of Cs (*6*–*8*) followed magnetic trapping approaches similar to those used before in the realization of BEC in Rb and Na (*14*, *15*). Resonant elastic scattering with a large cross section was observed, but a rapid loss of atoms due to inelastic two-body collisions had a detrimental effect on evaporative cooling and prevent-

Institut für Experimentalphysik, Universität Innsbruck, Technikerstraβe 25, 6020 Innsbruck, Austria.

ed the experiments from reaching BEC (*6*, *7*). More recent magnetic trapping experiments have explored a range of magnetic fields, where two-body loss is relatively small, and have approached the phase-space density required for BEC to within a factor of 10 (*13*).

The use of optical dipole forces allows atoms to be trapped in their lowest internal state (*25*), where the absence of internal energy leads to full suppression of inelastic two-body loss processes. Because atoms in this state seek out regions of high magnetic fields, they are in general not trappable by magnetic forces. Experiments in optical dipole traps (*9*–*12*) have explored cooling of Cs in the corresponding state, which has a total angular momentum $F = 3$ and a magnetic quantum number $m_F = 3$. Evaporative cooling (*12*) has approached BEC to within a factor of 2, before running into limitations by three-body processes (*26*).

Knowledge of the *s*-wave scattering length of the lowest internal state of Cs originates from precise measurements of low-field Feshbach resonances (*21*) and their theoretical analysis (*22*). The scattering length a shows a pronounced dependence on the magnetic field B (*27*, *28*): It varies from a large negative value at zero field ($-3000\ a_0$ at 0 G) to large positive values at higher fields (1000 a_0 at 55 G), going through zero at 17 G; $a_0 = 0.0529$ nm denotes Bohr's radius. This smooth variation over a wide magnetic field range can be interpreted as a result of a broad Feshbach resonance at about −8 G; here the negative field corresponds to a resonance position of +8 G (*22*) in the magnetically trappable state with $m_F = -3$. In addition to this broad one, several narrow Feshbach resonances occur (*27*, *29*), with the most prominent one at 48 G.

In our experiment, the starting point for evaporative cooling is a large-volume dipole trap that we realize by horizontally crossing two 100-W CO_2 laser beams (*30*). The trap has an effective volume of about 1 mm^3, is ~10 μK deep, and has a geometrically averaged trap frequency of $\bar{\omega}/2\pi = 14$ Hz. In contrast to the all-optical approach to BEC of (*31*), which uses tightly focused CO_2 laser beams and trap frequencies of the order of 1 kHz, our trap is shallow and designed for loading a large number of atoms rather than providing tight confinement. The CO_2 laser trap is loaded by adiabatical release of Cs atoms from an optical lattice. After Raman sideband cooling in the lattice according to (*32*) we start with a sample of 2×10^7 atoms with predominant polarization in the state $F = 3$, $m_F = 3$, a temperature of ~1 μK, and a phase-space density of a few 10^{-3}. Transfer losses and spatial mismatches, together with an excess potential energy of the trap, reduce the initial phase-space density to $\sim 10^{-4}$.

A magnetic levitation field (*30*) is applied to support the atoms against gravity (*12*, *14*). This field is essential to operate the large-volume CO_2 laser trap, which features optical forces far below the gravitational force on a Cs atom. Moreover, it is crucial for implementing efficient three-dimensional evaporation without being limited by gravitational sag. We combine the inhomogeneous levitation field with a freely adjustable bias field B_0 (*30*) to tune the scattering properties.

Evaporative cooling toward BEC proceeds in three stages (Fig. 1). In the first 10 s (Fig. 1A), the sample is cooled down by evaporation out of the CO_2 laser trap at constant trap depth. To obtain a sufficient collision rate at the rather low density of a few 10^{11} cm^{-3}, the scattering length is tuned to a large magnitude of $a = 1200\ a_0$ by setting the bias field to $B_0 = 75$ G. After 10 s, 2×10^6 atoms remain trapped at a temperature of ~1 μK and a phase-space density of about 10^{-3}.

In the following 5 s (Fig. 1B), an additional horizontal laser beam derived from a Yb fiber laser at a wavelength of 1064 nm is focused into the sample (waist, 30 μm) to create a narrow and deep potential well in the center of the CO_2 laser trap. Within these 5 s, the power is ramped up linearly from zero to 90 mW. The adiabatically deformed potential provides a strong local increase in the number density with a minor increase in the temperature, and a substantial gain in phase-space density is achieved (*33*, *34*). The magnetic bias field is set to $B_0 = 23$ G ($a = 300\ a_0$), which suppresses three-body loss as observed at higher values of a. Finally, one of the CO_2 lasers is turned off and about 3×10^5 atoms remain trapped in the combined field of the 1064-nm beam intersecting the CO_2 laser beam at an angle of 30°. This results in a cigar-shaped trap with tight radial confinement provided by the 1064-nm beam (radial trap frequency, 320 Hz). The axial confinement (axial frequency, 6 Hz) is essentially provided by the remaining CO_2 laser beam. In this way, a dense sample of Cs atoms (a few 10^{12} cm^{-3}) is prepared with a phase-space density on the order of 10^{-2}.

In the final stage (Fig. 1C), forced evaporative cooling is performed by ramping down the power of the 1064-nm beam to values of a few milliwatts within 17 s (*30*). The magnetic bias field is kept at 23 G ($a = 300\ a_0$), which is found to optimize the ratio of elastic collisions and inelastic three-body processes. We find that, for the given ramp, evaporative cooling toward BEC is possible only in a narrow magnetic field range between 21 and 25 G. Below 21 G, the cross

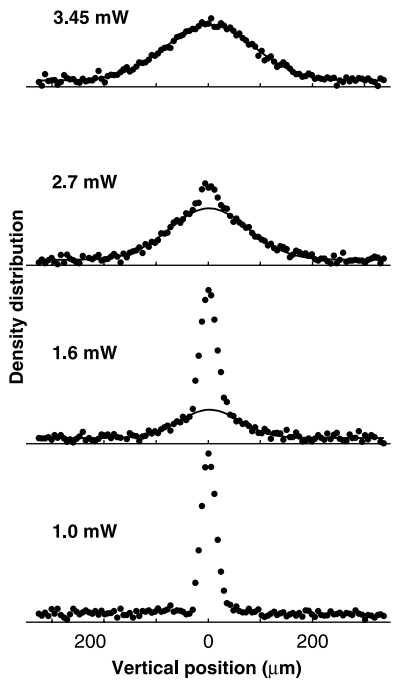

Fig. 2. Vertical density profiles of the released atom cloud observed after 50 ms of free expansion in the magnetic levitation field. The variable laser power at the end of the ramp is shown at left (in milliwatts). The profiles are obtained by horizontally integrating the measured column density in a 130-μm-wide region of interest. In these measurements, the magnetic bias field is switched to 17 G at the time of release to suppress the condensate expansion, which makes the appearance of the two-component distribution more pronounced. Gaussian fits to the thermal part of the distribution (solid lines in the upper three graphs) yield the temperatures.

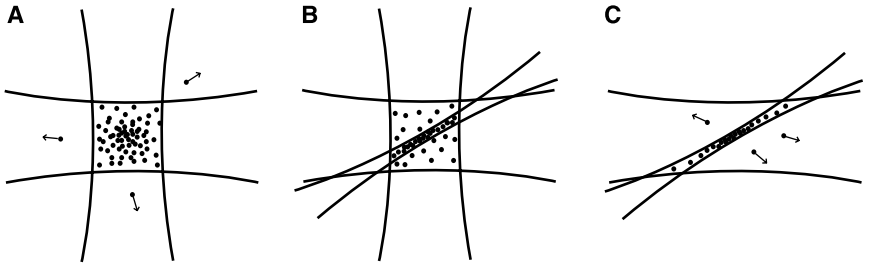

Fig. 1. Illustration of the three stages of evaporative cooling toward BEC of Cs. (**A**) Ten seconds of plain evaporation in two crossed CO_2 laser beams at a magnetic bias field of 75 G (scattering length tuned to 1200 a_0). (**B**) Five seconds of collisional loading of a tightly focused 1064-nm laser beam at 23 G (300 a_0). (**C**) Forced evaporative cooling by ramping down the power of the 1064-nm beam over 17 s, with the magnetic bias field kept at 23 G.

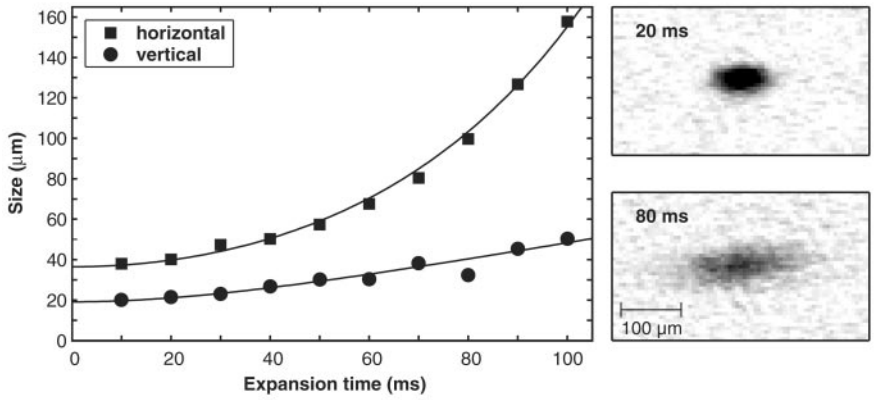

Fig. 3. Expansion of a non-interacting condensate at 17 G in the magnetic levitation field. The images at right show the condensate 20 ms (top) and 80 ms (bottom) after release. The data points at left show the 1/*e* half-widths of Gaussian fits to absorption images of the expanding cloud. The fit to the horizontal expansion shows the function $A\cosh(\alpha t)$, which describes the expansion with a calculated time constant of $\alpha^{-1} = 47$ ms (*30*) and an initial width $A = 36$ μm as the only adjustable parameter. The fit to the vertical expansion yields a mean kinetic energy of $k_B \times 600$ pK.

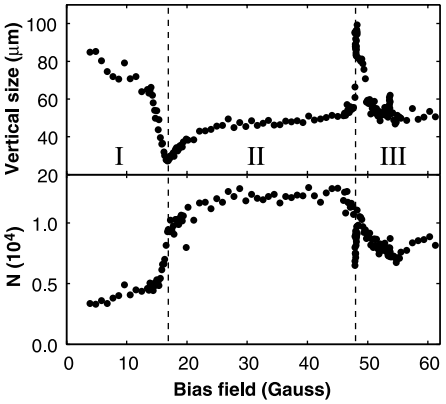

Fig. 4. Vertical extension (1/*e* half-width of a Gaussian fit) and atom number *N* of the expanding cloud as a function of the variable bias field applied in the first 10 ms after release. The measurements are taken after a total expansion time of 50 ms. The three different regions refer to (I) negative scattering length; (II) positive scattering length; and (III) a regime dominated by narrow Feshbach resonances, a prominent one at 48 G and a weaker one at 53 G.

section for elastic scattering is too small; and above 25 G, an increased rate of three-body processes in combination with the hydrodynamic collision regime leads to strong loss.

At the end of the ramp, the sample is released from the trap by simultaneously turning off both the CO_2 laser and the 1064-nm laser. In the magnetic levitation field, the atoms remain at a fixed vertical position. The observation time is typically limited to 100 ms by the horizontal spreading of the cloud that results from the weak transverse antitrapping force of the levitation field (*30*). For detection, absorption images are taken in a standard way (*14*, *15*) with a resonant probe beam that propagates horizontally at an angle of 30° with respect to the 1064-nm laser beam and 60° with respect to the CO_2 laser beam.

The BEC phase transition becomes obvious in the vertical density profiles of Fig. 2, which were taken 50 ms after release. Down to a final power of 3.45 mW (potential depth, 550 nK), a thermal cloud is observed; the corresponding profile shows a cloud of 65,000 atoms at temperature (T) = 46 nK. At final powers of 2.7 mW (450 nK) and 1.6 mW (260 nK), the profiles show a partially condensed cloud with T = 36 nK and 21 nK, respectively. At 1.0 mW (160 nK), an almost pure condensate is realized with 16,000 atoms. When the condensate with a peak density of 1.3×10^{13} cm^{-3} is kept in the trap, we measure a lifetime of ~15 s and infer an upper bound for the three-body loss coefficient of 2×10^{-27} cm^6 s^{-1}. This highlights the stability of the Cs BEC at the applied magnetic field.

We explore the magnetic tunability of the Cs condensate in the range between 5 and 65 G. The zero-crossing of the scattering length at 17 G allows us to turn off the self-interaction and thus to realize a "frozen" condensate with minimum internal energy. Figure 3 shows the measured expansion of the condensate, when B_0 is switched to 17 G at the time of release. In the vertical direction, a very slow expansion is observed, with a mean kinetic energy as low as $k_B \times 600$ pK (where k_B is Boltzmann's constant), which we attribute to residual self-interaction effects within the finite switching time. In the horizontal direction, the increasing width is fully determined by the horizontal magnetic force, which magnifies the initial cloud size according to the expected cosine hyperbolicus function (*30*). The non-interacting condensate can also be observed when the magnetic levitation field is turned off. Then, however, the observation of the falling BEC is limited to about 35 ms. We expect that with a few straightforward technical improvements in switching, the interaction energy of the "frozen" condensate could be reduced down to values of a few pK.

In order to demonstrate the other regimes of self-interaction, we switch to a variable magnetic field synchronously with the release of the condensate. The variable field is applied for a short time interval of 10 ms, which is sufficiently long for the mean-field dynamics to take place. For subsequent expansion at fixed conditions, the magnetic bias field is switched to 17 G. After a total expansion time of 50 ms, the vertical extension of the cloud and the total number of atoms are measured. The corresponding results (Fig. 4) show a marked dependence on the magnetic field with three distinct regions: Below 17 G (region I), the scattering length is negative and the BEC implodes, leading to a large momentum spread and a substantial loss of atoms. Between 17 and 48 G (region II), the scattering length is positive and varies smoothly from zero to about 1000 a_0. The expansion shows the minimum width at 17 G and a subsequent increase in width, in agreement with the predicted behavior of the scattering length. For higher fields (region III), the behavior is dominated by a narrow Feshbach resonance at 48 G. On this resonance, the cloud expands very rapidly as the condensate explodes in response to the strong sudden increase of its internal energy. In addition, a sharp loss feature is observed, which may indicate the formation of molecules in the BEC (*35*). At even higher fields, the data show an asymmetry and broadening of the resonance together with a loss of atoms, which we attribute to the finite ramp speed over the resonance (*17*).

The unique tunability offered by a Cs condensate is of great interest in various respects. In the field of quantum gases, it may serve as the experimental key to explore new regimes beyond standard mean-field theory, such as the strongly interacting regime with an interparticle spacing on the order of the scattering length, systems in reduced dimensionality, and the Mott insulator phase (*36*, *37*). Moreover, Cs is an interesting candidate for the creation of cold molecules and a molecular BEC (*35*, *38*). For applications in metrology, a "frozen" BEC without internal energy would represent an ideal source of cold atoms; for example, for precision measurements of the photon recoil (*39*). For future atomic clocks, one may envisage loading a very weak optical lattice with Cs atoms from a BEC. With one atom per site, such a system would provide long observation times with suppressed collisional frequency shifts.

Besides this particular interest in Cs, our experiments demonstrate that optical trapping methods allow BEC to be achieved with a species for which conventional magnetic trapping approaches have met severe difficulties.

References and Notes

1. C. Salomon *et al.*, *Proceedings of the 17th International Conference on Atomic Physics (ICAP 2000)*, E. Arimondo, P. D. Natale, M. Inguscio, Eds. (American Institute of Physics, Melville, NY, 2001), pp. 23–40.
2. J. M. Hensley, A. Wicht, B. C. Young, S. Chu, *Proceedings of the 17th International Conference on Atomic Physics (ICAP 2000)*, E. Arimondo, P. D. Natale, M. Inguscio, Eds. (American Institute of Physics, Melville, NY, 2001), pp. 43–57.
3. C. Chin, V. Leiber, V. Vuletic, A. J. Kerman, S. Chu, *Phys. Rev. A* **63**, 033401 (2001).
4. C. E. Wieman, *Proceedings of the 16th International Conference on Atomic Physics (ICAP 1998)*, W. E. Baylis, G. W. Drake, Eds. (American Institute of Physics, Woodbury, NY, 1999), pp. 1–13.
5. M. J. Snadden, J. M. McGuirk, P. Bouyer, K. G. Haritos, M. A. Kasevich, *Phys. Rev. Lett.* **81**, 971 (1998).
6. J. Söding, D. Guéry-Odelin, P. Desbiolles, G. Ferrari, J. Dalibard, *Phys. Rev. Lett.* **80**, 1869 (1998).
7. D. Guéry-Odelin, J. Söding, P. Desbiolles, J. Dalibard, *Europhys. Lett.* **44**, 26 (1998).
8. J. Arlt *et al.*, *J. Phys. B* **31**, L321 (1998).
9. H. Perrin, A. Kuhn, I. Bouchoule, C. Salomon, *Europhys. Lett.* **42**, 395 (1998).
10. A. J. Kerman, V. Vuletić C. Chin, S. Chu, *Phys. Rev. Lett.* **84**, 439 (2000).
11. D.-J. Han *et al.*, *Phys. Rev. Lett.* **85**, 724 (2000).
12. D. Han, M. T. DePue, D. Weiss, *Phys. Rev. A* **63**, 023405 (2001).
13. S. L. Cornish, S. Hopkins, A. M. Thomas, C. J. Foot, abstract from the 7th Workshop on Atom Optics and Interferometry, 28 September to 2 October 2002, Lunteren, Netherlands (book of abstracts).
14. M. Anderson, J. Ensher, M. Matthews, C. Wieman, E. Cornell, *Science* **269**, 198 (1995).
15. K. Davis *et al.*, *Phys. Rev. Lett.* **75**, 3969 (1995).
16. C. Bradley, C. Sackett, J. Tollett, R. Hulet, *Phys. Rev. Lett.* **75**, 1687 (1995).
17. S. Cornish, N. Claussen, J. Roberts, E. Cornell, C. Wieman, *Phys. Rev. Lett.* **85**, 1795 (2000).
18. G. Modugno *et al.*, *Science* **294**, 1320 (2001); published online 18 October 2001 (10.1126/science.1066687).
19. D. G. Fried *et al.*, *Phys. Rev. Lett.* **81**, 3811 (1998).
20. A. Robert *et al.*, *Science* **292**, 461 (2001); published online 22 March 2001 (10.1126/science.1060622).
21. C. Chin, V. Vuletic, A. J. Kerman, S. Chu, *Phys. Rev. Lett.* **85**, 2717 (2000).
22. P. J. Leo, C. J. Williams, P. S. Julienne, *Phys. Rev. Lett.* **85**, 2721 (2000).
23. L. Khaykovich *et al.*, *Science* **296**, 1290 (2002).
24. K. Strecker, G. Partridge, A. Truscott, R. Hulet, *Nature* **417**, 150 (2002).
25. R. Grimm, M. Weidemüller, Yu. B. Ovchinnikov, *Adv. At. Mol. Opt. Phys.* **42**, 95 (2000).
26. D. S. Weiss, personal communication.
27. A. J. Kerman *et al.*, *C. R. Acad. Sci. Paris IV* **2**, 633 (2001).
28. P. S. Julienne, E. Tiesinga, C. J. Williams, personal communication.
29. We observe the narrow Feshbach resonances at 11.0, 14.3, 15.0, 19.9, 47.7, and 53.4 G (accuracy ±0.2 G) as loss resonances in three-body decay of an uncondensed gas.
30. Materials and methods are available as supporting material on *Science* Online.
31. M. Barrett, J. Sauer, M. Chapman, *Phys. Rev. Lett.* **87**, 010404 (2001).
32. P. Treutlein, K. Y. Chung, S. Chu, *Phys. Rev. A* **63**, 051401 (2001).
33. D. Stamper-Kurn *et al.*, *Phys. Rev. Lett.* **81**, 2194 (1998).
34. M. Hammes, D. Rychtarik, H.-C. Nägerl, R. Grimm, *Phys. Rev. A* **66**, 051401(R) (2002).
35. E. A. Donley, N. R. Claussen, S. T. Thompson, C. E. Wieman, *Nature* **417**, 529 (2002).
36. D. Jaksch, C. Bruder, J. Cirac, C. Gardiner, P. Zoller, *Phys. Rev. Lett.* **81**, 3108 (1998).
37. M. Greiner, O. Mandel, T. Esslinger, T. W. Hänsch, I. Bloch, *Nature* **415**, 39 (2002).
38. F. Masnou-Seeuws, P. Pillet, *Adv. At. Mol. Opt. Phys.* **47**, 53 (2001).
39. S. Gupta, K. Dieckmann, Z. Hadzibabic, D. E. Pritchard, *Phys. Rev. Lett.* **89**, 140401 (2002).

40. We thank all members of the cold-atom group for support and a great team spirit. In particular, we thank the Cs surface trapping team, M. Hammes, D. Rychtarik, and B. Engeser, for fruitful interactions and for sharing the 1064-nm laser; A. Noga for assistance; and J. Hecker Denschlag for useful discussions. We are indebted to R. Blatt and his ion trapping group for support during our start-up phase in Innsbruck. We acknowledge financial support by the Austrian Science Fund (FWF) within project P15114 and within SFB 15 (project part 16).

Supporting Online Material
www.sciencemag.org/cgi/content/full/1079699/DC1
Materials and Methods
Figs. S1 to S3
References

23 October 2002; accepted 26 November 2002
Published online 5 December 2002;
10.1126/science.1079699
Include this information when citing this paper.

Anthropogenic CO_2 Uptake by the Ocean Based on the Global Chlorofluorocarbon Data Set

Ben I. McNeil,[1]* Richard J. Matear,[2] Robert M. Key,[1] John L. Bullister,[3] and Jorge L. Sarmiento[1]

We estimated the oceanic inventory of anthropogenic carbon dioxide (CO_2) from 1980 to 1999 using a technique based on the global chlorofluorocarbon data set. Our analysis suggests that the ocean stored 14.8 petagrams of anthropogenic carbon from mid-1980 to mid-1989 and 17.9 petagrams of carbon from mid-1990 to mid-1999, indicating an oceanwide net uptake of 1.6 and 2.0 ± 0.4 petagrams of carbon per year, respectively. Our results provide an upper limit on the solubility-driven anthropogenic CO_2 flux into the ocean, and they suggest that most ocean general circulation models are overestimating oceanic anthropogenic CO_2 uptake over the past two decades.

Despite improvements in our understanding of the partitioning of anthropogenic CO_2 between the atmosphere, ocean, and terrestrial biosphere, substantial uncertainties and insufficient direct observational constraints continue. Recent decadal-scale changes in oxygen concentrations that have been observed in the ocean (*1*, *2*) imply large and uncertain corrections (*3*–*5*) to the oceanic and terrestrial sinks for anthropogenic CO_2 that have been estimated based on atmospheric O_2/N_2 observations (*6*, *7*), which was the method used in the 2001 report by the Intergovernmental Panel on Climate Change (*8*). Because the O_2/N_2 technique is based on atmospheric observations, it inherently requires assumptions regarding the partitioning of anthropogenic CO_2 between the ocean and terrestrial biosphere. Ocean general circulation models (OGCMs) currently simulate oceanic anthropogenic CO_2 uptake, assuming a steady-state circulation and biological production (*9*). We present here an observational estimate of the decadal inventory of anthropogenic CO_2 in the ocean based on the global chlorofluorocarbon (CFC) data set. Our estimates provide independent observational insights into the contemporary global carbon budget and provide a framework that can be used for direct validation of ocean model predictions.

The most direct way of estimating anthropogenic CO_2 accumulation in the ocean is to compare dissolved inorganic carbon (DIC) measurements made at one time with those made later in the same region. To isolate the long-term trend from changes due to natural variability, DIC measurements along isopycnal surfaces (*10*) can be compared, or multiple linear regression (MLR) of DIC against hydrographic properties (*11*) can be used (Fig. 1C legend). Although these methods provide direct evidence for regional anthropogenic CO_2 accumulation (*10*, *12*, *13*), they currently cannot be used in the global context because of the lack of adequate historical DIC measurements.

Another way to estimate anthropogenic CO_2 is to study the distribution of CFCs in the ocean. The release of CFC-11 (CCl_3F) and CFC-12 (CCl_2F_2) to the atmosphere began in the 1930s and accelerated in the 1950s. CFCs are entirely anthropogenic and biologically inert in the ocean. The oceanic CFC distribution thus provides valuable information about the rates and pathways of water mass ventilation processes (*14*). As part of the World Ocean Circulation Experiment (WOCE) carried out in the 1990s, dissolved CFCs were measured with great accuracy and unprecedented global resolution (Fig. 2). The patterns of oceanic accumulation

[1]Atmospheric and Oceanic Science Program, Princeton University, Princeton, NJ 08544, USA. [2]Commonwealth Scientific and Industrial Research Organisation Marine Research and the Antarctic Co-operative Research Centre, Hobart, Tasmania, Australia. [3]Pacific Marine Environmental Laboratory, National Oceanic and Atmospheric Administration, Seattle, WA 98115, USA.

*To whom correspondence should be addressed.